



HAL
open science

In-vessel corium thermochemistry benchmark based on MASCA-CORDEB2 experimental data

Romain Le Tellier, Laure Carénini, Florian Fichot, Rositsa Gencheva, Pavlin Groudev, Ivan Melnikov, M. Golubev, Aleksandr Filippov

► **To cite this version:**

Romain Le Tellier, Laure Carénini, Florian Fichot, Rositsa Gencheva, Pavlin Groudev, et al.. In-vessel corium thermochemistry benchmark based on MASCA-CORDEB2 experimental data. ERMSAR 2024 - 11th European Review Meeting on Severe Accident Research Conference, May 2024, Stockholm, Sweden. pp.ID78. cea-04838611

HAL Id: cea-04838611

<https://cea.hal.science/cea-04838611v1>

Submitted on 14 Dec 2024

HAL is a multi-disciplinary open access archive for the deposit and dissemination of scientific research documents, whether they are published or not. The documents may come from teaching and research institutions in France or abroad, or from public or private research centers.

L'archive ouverte pluridisciplinaire **HAL**, est destinée au dépôt et à la diffusion de documents scientifiques de niveau recherche, publiés ou non, émanant des établissements d'enseignement et de recherche français ou étrangers, des laboratoires publics ou privés.

IN-VESSEL CORIUM THERMOCHEMISTRY BENCHMARK BASED ON MASCA EXPERIMENTAL DATA

R. Le Tellier

CEA, DES, IRESNE, DTN, Cadarache
F-13108 Saint Paul-lez-Durance, France
romain.le-tellier@cea.fr

L. Carénini, F. Fichot

IRSN, Cadarache
F-13108 Saint Paul-lez-Durance, France
laure.carenini@irsn.fr, florian.fichot@irsn.fr

R. Gencheva, P. Groudev

Institute for Nuclear Research and Nuclear Energy – Bulgarian Academy of Sciences, INRNE-
BAS
72 Tsarigradsko shosse Blvd. BG-1784 Sofia, Bulgaria
r.gencheva@inrne.bas.bg, pavlinpg@inrne.bas.bg

I. Melnikov, M. Golubev

NRC “Kurchatov Institute”
1 Akademika Kurchatova Pl., RU-123182 Moscow, Russia
Melnikov_IA@nrcki.ru

A. Filippov

IBRAE
52 B. Tulsкая St. RU-115191 Moscow, Russia
phil@ibrae.ac.ru

ABSTRACT

This paper presents the first two steps of a benchmark on in-vessel corium thermochemistry, which is part of the IAEA Coordinated Research Project on In-Vessel Melt Retention. The benchmark focuses on the stratification of corium in the lower plenum of a reactor vessel during a severe accident. The experimental data from the MASCA test facilities are used to validate/calibrate the models of the different codes used by the participants. The paper gives an overview of the different models, including their underlying assumptions. The results show that the models are generally in good agreement with the experimental data, but further experimental data is needed for model validation. Besides the need for further work, this paper highlights the fact that integral models (published in the open literature for most of them) are available to account for the first-order phenomena associated with in-vessel corium. Accordingly, this paper may be useful for code developers that would like to upgrade their models in order to take into account transient stratification kinetics, a prerequisite for a state-of-the-art analysis of in-vessel melt retention.

KEYWORDS

corium, thermochemistry, stratification, benchmark

1. INTRODUCTION

In the framework of the IAEA Coordinated Research Project (CRP) on In-Vessel Melt Retention*, a code-to-experiment benchmark devoted to in-vessel corium thermochemistry was proposed by CEA and IRSN with participation from IRNRE-BAS, NRC “Kurchatov Institute” and IBRAE. Based on results of prototypic corium experiments from the open literature, it is devoted to oxide/metal pool thermochemistry phenomena of first-order importance when assessing in-vessel corium behavior [1]. Indeed, as clearly demonstrated by the H2020 IVMR European project, taking into account the transient multilayer corium configuration in the vessel lower head is mandatory for assessing In-Vessel Retention (IVR) for high power reactors.

It is a three-step benchmark involving both severe accident codes (ASTEC, HEFEST-URAN, HEFEST) and thermodynamic equilibrium solvers (TSAR, OpenCalphad) with associated databases (NUCLEA).

The first step considers two-layer stationary (under chemical equilibrium conditions) pool configurations using oxide/metal phases’ composition and relative position information taken from the MASCA-MA tests series [2]. It is used for comparison and validation of the modelling of the liquid miscibility gap of the U-O-Zr-steel thermodynamic system and the liquid phase density laws. The second step is focused on the heavy metal layer formation kinetics considering the last phase of the MASCA-RCW experiment and associated post-mortem ingot information [3]. Here, a semi-quantitative comparison with experimental results (in terms of metal phase spatial distribution and composition) is performed in order to assess intra-layer mass transfer models that simulate corium stratification transients in severe accident codes. In this second step, the light metal layer and the oxide phase are not separated by a solid crust contrarily to the reactor case. In the third step, it is the transient evolution of a three-layer stratified corium pool in presence of a solid crust at the top oxide surface that is studied considering the results of CORDEB2 CP7-02 test on the stratification kinetics [4]. In this experiment, the thermal gradient expected in reactor configuration leading to crust formation between the oxide and the top metal layer is considered, albeit in a small geometry for which the crust is mechanically stable.

This paper presents the specifications of the first two steps of this benchmark along with an analysis of the results obtained by the participants.

2. STEP 1: MASCA MA

2.1. Brief summary of the experiments

The OECD-MASCA experimental program (see [2]) has studied the thermochemical interactions between an oxide phase and a metallic phase. Among other achievements, it has helped characterizing the (U, Zr) mass transfer to the metal phase that can lead to a significant increase in its density so that, in some conditions, the metal phase can be relocated at the bottom of the pool because of gravity.

In particular, some experiments of the MA series (MA-1 to MA-6), under inert atmosphere in the RASPLAV-3 facility (NITI), have shown, both through direct observation of the free surface during the experiment and by post-mortem analyses of the solidified ingots, the possibility of two stratified configurations at steady-state. These experiments were conducted using the cold-crucible technique to melt about 2kg of oxidic corium by inductive heating in a 7cm-diameter crucible. Steady state was reached in any case in less than 30min.

The MA series partial test matrix is given at Table I in terms of the melt temperature T^{exp} , the exposure time, the suboxidized corium initial composition (defined by its U-over-Zr molar ratio $R_{U/Zr}$ and the Zr

* <https://www.iaea.org/projects/crp/j46002>

molar oxidation degree C_{Zr}) and the ratio between the steel mass and the initial corium mass (denoted x_{steel}^{exp}).

Note that Table I give the specified test conditions; actual molten masses at play in the corium-steel interactions slightly differ.[†]

The post-mortem ingots analysis gives information about the phases stratification as illustrated in Figure 1. For the MA-1, MA-3, MA-4, MA-5, MA-5b tests, a clear stratification with a metal phase heavier than the oxide has been observed while the metal phase is lighter and on top of the oxide in the MA-6 test.

■ **Nota Bene** The MA-2 test with a highly oxidized corium ($C_{Zr}^{exp} = 74.5\%$) is the only test that does not exhibits a clear phase stratification. In this case, the metal phase is inhomogeneous and has a “diabolo” shape with a top (resp. bottom) part that is lighter (resp. heavier) with a density of 7930 kg/m³ (resp. 8890 kg/m³) than the oxide phase (8610 kg/m³). Obviously, an equilibrium calculation cannot reproduce or explain such a configuration. Different supplementary explanations (magneto-hydrodynamic effects associated with the inductive heating, helicoidal shrinkage during solidification, complicated phase segregation during solidification - possibly largely impacted by oxygen redistribution) have been proposed in the literature; they are out of the scope of this benchmark. ■

Table I. MA series partial test matrix.

Test	T^{exp} (°C)	Exposure time (min)	$R_{U/Zr}^{exp}$	C_{Zr}^{exp} (%)	$\frac{x_{steel}^{exp}}{x_{steel}^{exp}+1}$ (%)
MA-1	2500	30	1.45	33.1	11.42
MA-2			1.28	74.5	10.80
MA-3			1.14	36.5	10.78
MA-4			1.17	39.7	19.09
MA-5			0.89	31.5	9.89
MA-5b		120	0.90	30.5	7.05
MA-6	2600	30	1.14	29.1	29.71

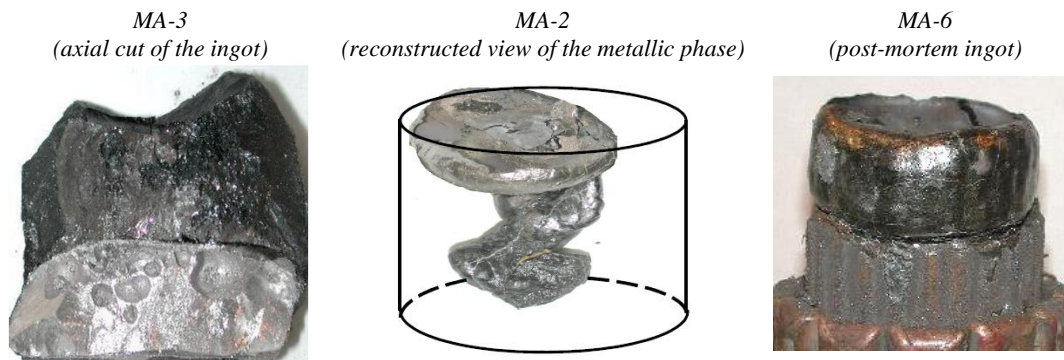


Figure 1. Different views associated with the post-mortem ingots of MA-3, MA-2 and MA-6 tests (adapted from [2]).

[†] Moreover, in MA-3 and MA-4 tests, the corium load contained fission products (FP) simulant elements with a mass fraction of about 3%. The goal was to characterize the FP partitioning between the metal and oxide phases. These elements are not considered in the first step of this benchmark.

2.2. Benchmark definition

The objective is to compare both the experimental results (associated with the post-mortem ingots analyses) and numerical results obtained by different models that predict the two-phase thermodynamic equilibria in the liquid miscibility gap of the U-O-Zr-steel system. These calculations are performed from the element inventories deciphered from the actual molten masses as evaluated from post-mortem test analyses in [5].[‡] They are given in Table II.

Table II. Inventory considered in the different MA tests.

Test	Mass (kg)	Element mass fractions					
		<i>U</i>	<i>Zr</i>	<i>O</i>	<i>Fe</i>	<i>Ni</i>	<i>Cr</i>
MA-1	1.620500	0.6180692	0.1631392	0.1062624	0.0774678	0.0124510	0.0226104
MA-2	1.749200	0.5898773	0.1760788	0.1266666	0.0743082	0.0113718	0.0216974
MA-3	1.648984	0.5871907	0.1967083	0.1063043	0.0846189	0.0098253	0.0153524
MA-4	1.828151	0.5393137	0.1757293	0.0910485	0.1390972	0.0196035	0.0352079
MA-5	1.913298	0.5592548	0.2417220	0.1010353	0.0705727	0.0107234	0.0166917
MA-5b	1.914332	0.5780783	0.2470213	0.1052485	0.0521638	0.0099463	0.0075419
MA-6	1.836680	0.4693826	0.1572136	0.0780316	0.2104556	0.0321988	0.0527179

For each experiment, two different calculations are performed:

- C1. A first one at the composition given in Table II that is used for direct comparison with the experimental results in terms of element phases partitioning;
- C2. A second one where, the composition given in Table II is varied in terms of steel amount near x_{steel}^{exp} ($R_{U/Zr} = R_{U/Zr}^{exp}$ and $C_{Zr} = C_{Zr}^{exp}$ are kept); more precisely, five calculations with $x_{steel} \in \{0.75, 0.875, 1.0, 1.125, 1.25\} \times x_{steel}^{exp}$ are performed in order to characterize the evolution of the mass densities.

Regarding the temperature, while the different species phase partitioning models are or not temperature dependent, the mixture density laws are in any case temperature dependent. For calculation C1, the temperature is set to $T_{calc} = \max(T^{exp}, T_{liquidus})$, where $T_{liquidus}$ is the liquidus temperature (calculated by the model if available) at which the fluorite refractory phase $(U_y, Zr_{1-y})O_{2-x}$ is formed when the melt is cooled down (assuming thermodynamic equilibrium). For calculations C2, a temperature of $T^{exp} + 100^\circ$ is used in order to ensure that, for all compositions when varying x_{steel} , the system remains into the liquid miscibility gap.[§]

2.3. Codes and models involved

Different thermodynamic equilibrium models for the liquid miscibility gap of the U-O-Zr-Steel system are used by the participants through different codes as described in Table III. These different models provide the phase mass fractions along with their composition. From there, the phase densities are calculated from:

- a non-ideal mixture law based on element density laws and an excess volume term function of the temperature (see [6]) in NRC “Kurchatov Institute” and IBRAE calculations;

[‡] Inventories reported in [5] differs from those in [2] because of more accurate measurements of the oxygen content in the metallic layers.

[§] Then, one should keep in mind that the densities will be lower than in C1 calculations.

- an ideal mixture law based on species density laws function of the temperature $\rho_i(T)$ (see [7]) in case of IRSN, INRNE-BAS and CEA calculations.

The parameters of these laws are code/model dependent and are based on different experimental results compiled in different databases. In the case of CEA calculations, the laws proposed in [7] were used (even if there are not the default ones considered in PROCOR) considering two treatments when, for a given species i , the mixture temperature T is below the species liquidus temperature $T_i^{liquidus}$: either $\rho_i(T < T_i^{liquidus})$ is set to $\rho_i(T_i^{liquidus})$ (M1 hypothesis) or it is extrapolated (M2 hypothesis).

Table III. The different codes and models for the liquid miscibility gap of the U-O-Zr-Steel system involved in step-1.

Institution	N°	Code / model	Description/comments	Ref.
NRC “Kurchatov Institute”	1	TSAR / GIBBS	Thermodynamic approach based on Gibbs energy minimization using regular solution model (CALPHAD-like technique)	[8]
IRSN	2	ASTEC / Salay-Fichot model	Analytical model calibrated on experimental results from MASCA MA-1, 2, 3, STFM-Fe-2, 3, 4, 5, 6, 7, 8, 9, 14, 15	[9]
INRNE-BAS	3			
IBRAE	4	HEFEST_URAN	Interpolation scheme based on MASCA MA and STFM-Fe test experimental results	[10]
CEA	5	PROCOR interface with OpenCalphad / Gibbs energy minimizer with NUCLEA'19 database	CALPHAD method with a non-ideal associate model for the Gibbs energy of the liquid phase	[11] [12]
	6	PROCOR / Salay-Fichot model	See ASTEC above	[9]
	7	PROCOR / Nandan-Fichot model	Analytical model calibrated on OpenCalphad calculations with NUCLEA'19 database	[13]
	8	PROCOR / thermodynamic closures associated with the stratification kinetics model proposed in [14]	Interpolation scheme based on OpenCalphad calculations with NUCLEA'19 database	[14]

2.4. Results comparison and analysis

Results for the C1 calculations are presented in Table VI as a comparison with the experimental values in terms of the oxide phase mass fraction (w^{oxy}), the uranium (resp. zirconium) mass fraction in the metal phase w_U^{met} (resp. w_{Zr}^{met}). It can be observed that, in most cases, the relative discrepancy associated with the phase partitioning (in terms of oxide phase mass fraction) is less than 10%. For calculations based on the NUCLEA database (n°5 and, through fitting/interpolation, n°7 and 8), results are deteriorated in MA-6 conditions *i.e.* with a higher x_{steel}^{exp} value. The same comment applies to Salay-Fichot models based results n°6, 2 and 3** along with IBRAE result n°4. Regarding the metal phase enrichment in Zr, it is underestimated in most calculations in MA-3, 4, 5, 5b, 6 conditions. Note that it is worst in results n°2, 3, 6 and 7 because of the underlying hypothesis of the Salay-Fichot and Nandan-Fichot models that considers the $R_{U/Zr}$ ratio as uniform between the two phases while actually, it significantly decreases in the metal phase at equilibrium

** Note that ASTEC results obtained independently by IRSN and INRNE are almost the same while, apparently, the Salay-Fichot model implemented in PROCOR differs significantly from the one in ASTEC code.

(i.e. Zr is preferentially extracted in the metal phase). Only result n°1 shows a limited Zr underestimation in these five tests. In MA-1 (higher $R_{U/Zr}$ w.r.t. MA-3) and MA-2 (higher C_{Zr} w.r.t. MA-3) conditions, calculations 1 and 5 are consistent with a significant overestimation of the Zr content (a compensation effect can be observed for results n°2, 3, 6 and 7 because of the previously mentioned hypothesis). Regarding result n°8, because of the way the interpolation scheme is constructed (see [14]), it gives consistent results w.r.t. result n°1 in terms of w^{oxy} and w_{Zr}^{met} and about 10% difference in w_{U}^{met} in all cases.

On the overall, considering the fact that these tests are not strictly at thermodynamic equilibrium and the underlying experimental uncertainty, it is worth noting that the results based on a thermodynamic database with a Gibbs energy minimizer (n°1 and 5) are in fairly good agreement.

Regarding C2 calculations, the oxide (resp. metal) phase density ρ^{oxy} (resp. ρ^{met}) as a function of x_{steel} is depicted in the MA-1 (heavier metal) and MA-6 (lighter metal) cases in Figure 4 (resp. Figure 5) while the phase density differences $\rho^{met} - \rho^{oxy}$ [kg.m⁻³] for $x_{steel} = x_{steel}^{exp}$ are given for all the cases in Table VII. For this second set of calculations, PROCOR results are only shown with the Salay-Fichot equilibrium model (n°6) with the two different hypotheses (denoted M1 and M2) regarding the density calculation introduced in §2.3. It can be observed that, as expected, these hypotheses have only an impact on the oxide phase density. Moreover, using M1 (resp. M2), the oxide mass density calculated by PROCOR is rather consistent with result n°1 by NRC KI (resp. n°2 by IRSN). In all cases, result n°4 by IBRAE exhibits a significantly higher oxide density. In the case of INRNE result (n°3), they were performed at a lower temperature in such a way that, compared with result n°2 (that uses the same ASTEC code), a higher oxide density is obtained. Regarding the metal density, result n°4 gives lower density than results n°2 and 6 while calculation n°1 gives a higher (resp. lower) density for a low (resp. high) x_{steel} value as in MA-1 (resp. MA-6) conditions. On the overall, when looking at the phase density differences, PROCOR results with M2 hypothesis, ASTEC results produced by IRSN and NRC-KI results are rather close with a difference in magnitude that is comparable with the temperature effect that can be quantified when comparing ASTEC results between IRSN and INRNE. The calculations that give difference that is more significant are the ones produced by IBRAE with HEFEST_URAN.

These density differences would need further analysis going back to the density laws implemented in the different codes that may not be at the state-of-the-art (this comment applies to PROCOR based on TOLBIAC-ICB physical properties laws for instance) taking into account recent experimental data.

3. STEP 2: MASCA RCW-100

3.1. Brief summary of the experiment

In the OECD-MASCA experimental program [2], one prototypical experiment of larger scale than the previous MA tests has been conducted and is of interest for characterizing the stratification transient. It is the MASCA-RCW test [3] where 45.3kg of suboxidized corium has been put in interaction with about 4.6kg of steel (in such a way that the global system is, in terms of thermodynamic equilibrium, below the stratification inversion threshold). This experiment was carried out in a cold crucible of about 18cm-diameter. It was interrupted after 22min of interaction between molten corium and molten steel poured on top and the analysis of the post-mortem ingot clearly shows that the system has not reached a stationary state with two stratified layers. The vertical cross-section of the ingot is shown in Figure 2. The interpretation proposed in [15] consists in considering this post-mortem ingot as the solidified state of the system during the transient relocation of steel below the oxide; the metal phases are spatially distributed as follows:

- a continuous light metal phase (7) above the oxide pool (5);
- a dispersed metallic phase enriched in U and Zr that can be viewed as centimetric droplets^{††} (4) relocating downward through oxide (5);

^{††} In the post-mortem state, internal porosities can be observed in these droplets. The SEM/EDX composition analysis reveals that they were probably filled by CO gas (traces of Zr(O_{0.14}C_{0.85}) are found at the interface). Accordingly, as

- a continuous heavy metal phase (2) below the oxide (5).

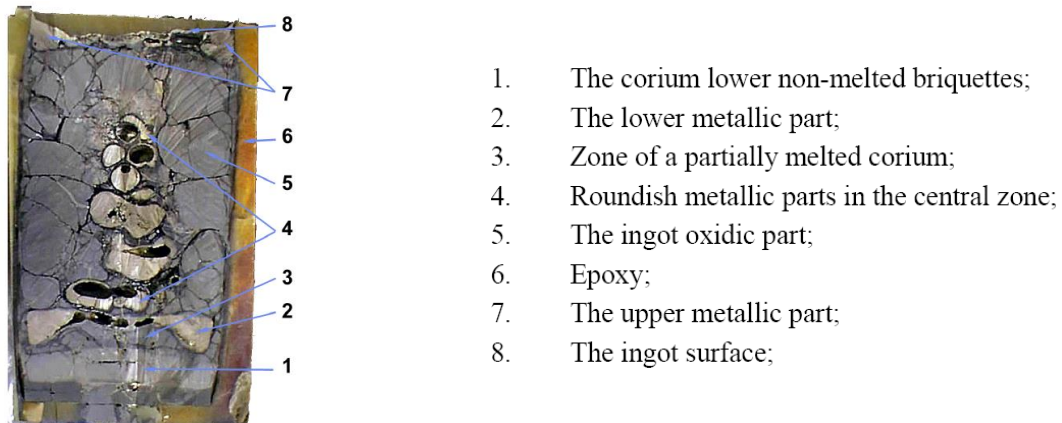


Figure 2. Vertical cross-section of the MASCA-RCW post-mortem ingot (adapted from [2]) – diameter ~18cm and height ~26cm – without (1).

From there, two mechanisms are at play, as discussed in [15]. First, there is a transfer of U and Zr from the oxide to the steel (associated with modification of the redox equilibrium $U + ZrO_2 \leftrightarrow UO_2 + Zr$) that induces local changes in mass density. Then, when the metal in the boundary region becomes “sufficiently” heavier than the oxide, the triggering and growth of Rayleigh-Taylor instabilities at the interface between the light metal layer and the oxide lead to the formation and detachment of heavy metal droplets that sink through the oxide (and form a continuous heavy metal phase at the bottom). These hydrodynamic phenomena appear to be periodic in nature and are much faster than the bulk transport of components within the light metal layer. Indeed, as shown in Figure 3, the U, Zr components in the light metal phase are concentrated in a boundary region near the interface.

This interpretation was used in the construction of the legacy PROCOR stratification model [17] (originating from the modelling hypotheses proposed in [15]) where the overall kinetics is supposed to be controlled by the interlayer mass transfer (the hydrodynamic phenomena are not modelled).

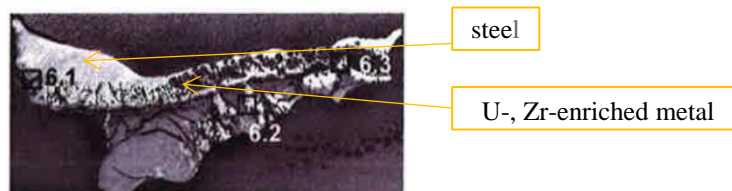


Figure 3. Microscopic structure of the solidified light metal phase of the MASCA-RCW post-mortem ingot (adapted from [2]) – dimensions ~9x4cm.

3.2. Benchmark definition

The objective is to compare both the experimental results (associated with the post-mortem ingots analyses) and numerical results obtained by different models that simulate such a stratification transient where, from a two-layer pool with steel on the top, a heavy metal phase is formed.

mentioned in [3], it is considered that this gas formation is associated with the decrease of the oxygen solubility in metal when solidification took place and CO was formed by the interaction between this oxygen and carbon coming from the steel. Accordingly, at liquid state, no gas is expected.

Because of the complexity of such an experiment and the fact that, from the point of view of phases stratification, only indirect post-mortem data are available, the considered simulation set-up is actually an idealized two-layer configuration representative of the system state after the corium has been melted and the molten steel has been poured on top.

Accordingly, the code-to-experiment comparison can only be semi-quantitative but, considering the level of uncertainty of this stratification issue, it is the authors' point of view that such a comparison (and the associated code-to-code comparison) is still very valuable.

The initial state of the two-layer system given in Table IV is considered in a geometry consisting in a 9-cm cylinder. From there, the time-dependent spatial distribution of the phases is simulated until steady-state has been reached.

This initial inventory was constructed back from the inventory of the different phases in the post-mortem that is used for comparison with simulation results at time $t=22\text{min}$.

During these 22min of interaction between molten steel and molten corium, the thermal power deposited into the melt was about 25kW while the liquidus temperature of the overall system is about 2500°C.

Table IV. Inventory considered in the RCW-100 test.

Phase α	Mass (kg)	Species mass fraction (%)					
		UO ₂	Zr	ZrO ₂	Fe	Cr	Ni
Steel	3.989	0.0	0.0	0.0	69.64291	16.22873	14.12836
Oxide	48.781	76.25693	14.24420	0.949887	0.0	0.0	0.0

■ **Nota Bene** The first phase of the experiment (corium melting), while not the focus of this benchmark, is also of interest for code validation as demonstrated by supplementary calculations (not shown here) performed by IBRAE with HEFEST_URAN in the frame of this collaborative work. ■

3.3. Codes and models involved, main parameters selection

The different stratification kinetics models used by the participants through different codes are described in Table V.

Note that in most of these models, the detachment of U-/Zr- enriched metal from the upper metal phase under the form of droplets (that relocate downwards to form the heavy metal phase formation) is based on a simple density difference criterion between the interfacial enriched metal and the oxide. In addition, it should be noted that only the model associated with result n°5 explicitly takes into account the metal droplets and their relocation; in other models, the time for relocation is neglected.

In all these models, the main important parameters (either effective diffusion coefficients or mass transfer coefficients) are related to the inter-layer mass transfer kinetics and they have been approximately calibrated so that the mass of the heavy metal phase at $t=22\text{min}$ is in good agreement with the experiment. In addition, for result n°5, the model parameters were selected so that the first droplet detachment occurs slightly before $t=22\text{min}$ in accordance with the measurements during the experiment that show a rapid increase in the temperature at the bottom of the crucible slightly before the power was shutdown, indicating a change in the melt phase topology. This model calibration is not further discussed for the sake of conciseness.

Table V. The different codes and models for the stratification kinetics involved in step-2.

Institution	N°	Code / model	Description/comments	Ref.
IRSN	1	ASTEC / inter-layer mass transfer model	Mass transfer considered simultaneously at the two interfaces upper metal/oxide, oxide/lower metal; local interface equilibrium approximated by the thermochemical equilibrium (Salay-Fichot model, see n°2/3 in Table III) of the two phases at this interface	[16]
INRNE-BAS	2			
IBRAE	3	HEFEST_URAN / MultiMelt module	1D finite element diffusion model for uranium in the upper metal phase	-
CEA	4	PROCOR / legacy inter-layer mass transfer model	Evolution equation for the uranium mass fraction in the oxide phase considering the exchange with the upper metal phase; degree of advancement towards global thermochemical equilibrium (Salay-Fichot model, see n°6 in Table III)	[17]
	5	PROCOR / “new” integral mass transfer model that takes into account the dispersed metal phase (mass transfer and dynamics)	Mass and element mass conservation for all phases; interface jump conditions associated with local equilibrium simplified under the hypothesis that there is no oxygen (resp. steel) in the metal (resp oxide) phases; thermodynamic closures: see n°8 in Table III; 1D droplet momentum conservation equation	[18] [19] [14]

3.4. Results comparison and analysis

The results for the different codes are given in Figure 6 in terms of the oxide (m^{oxy}) and heavy metal phase ($m^{met\downarrow}$) masses as a function of time along with the evolution of the U ($w_U^{met\downarrow}$) and Zr ($w_{Zr}^{met\downarrow}$) mass fractions in the heavy metal phase. Values associated with post-mortem analyses of the experiment ingot (metal phases) are also depicted at $t=22\text{min}$ for comparison purpose. More precisely, three values are depicted for $m^{met\downarrow}$, $w_U^{met\downarrow}$ and $w_{Zr}^{met\downarrow}$ considering:

- the actual heavy metal phase below the oxide ($met \downarrow$);
- the actual heavy metal phase ($met \downarrow$) plus the droplets inside the oxide ($drop \downarrow$);
- the actual heavy metal phase ($met \downarrow$) plus the droplets ($drop \downarrow$) plus the U-, Zr-enriched boundary region of the light metal layer ($\widetilde{met} \uparrow$).

The following general trends can be observed on the phase masses evolution. In results n°1, 2, and 4, the formation of the heavy metal phase is described continuously (as the underlying models do not intend to capture the discontinuous nature of the process associated with the Rayleigh-Taylor instabilities) and starts from $t=0\text{s}$. In result n°3, the heavy metal formation starts around 800s and then steadily increases by further continuous relocation from the light metal layer. In result n°5, a first droplets detachment occurs just around 1310s to form the heavy metal layer which mass then slowly increases by mass transfer through its interface with the oxide phase until the next droplet detachment (not shown in Figure 6, that occurs around 2750s). As expected, the different models having been approximately calibrated, their prediction of the heavy metal mass at 22min is fairly good.

When looking at the evolution of the U and Zr mass fractions in the heavy metal layer in Figure 6, further remarks can be made. First, in PROCOR legacy model, because of the underlying modelling hypotheses, the heavy metal phase composition is constant in time, set to its value at global thermochemical equilibrium. With ASTEC model (in both IRSN and INRNE calculations that are almost undistinguishable), this composition in U and Zr exhibits a rapid increase starting after 200s and then a slow decrease towards its global equilibrium value. At the experiment exposure time, for both models, the U mass fraction is approximately reproduced while the Zr mass fraction is underestimated; this is consistent with the trends observed with the Salay-Fichot equilibrium model in both codes in Table VI for MA-3 conditions (close to

RCW global inventory). Second, in PROCOR “new” model, looking at the heavy metal phase composition when it is formed around 1310s, the opposite trend is observed consistently with the observations made in Table VI in MA-3 conditions for result n°8. After its formation, the U and Zr content of the heavy metal phase increases by mass transfer through its interface with the oxide phase. Third, in IBRAE calculation, the heavy metal formed around 650s exhibits a high U and Zr content that rapidly decreases (by further addition of metal relocated from the light metal layer) ; at the experiment exposure time, the U mass fraction is approximately reproduced while the Zr mass fraction is underestimated.

While this experiment offers a unique qualitative comparison for stratification kinetics and can be used for calibration purpose, it appears clearly that additional experimental results are needed to go further in the model validation as already stated in [20].

4. CONCLUSIONS AND PERSPECTIVES

In this paper, the first two steps of a benchmark devoted to in-vessel corium thermochemistry have been presented both in terms of test specifications and results obtained so far by the participants involved in the frame of the IAEA CRP on In-Vessel Melt Retention. The first step, based on the MASCA MA experiment series, has highlighted the overall good capability of either simple models published in the open literature or thermodynamic equilibrium calculations (based on a thermodynamic database and a Gibbs energy minimizer) to evaluate the mass and species partitioning of the two-layer pool at steady-state. It has also shown discrepancies among codes regarding the phase density evaluation that would require further analysis and comparison with state-of-the-art experimental measurements of such mixture densities. Considering the MASCA RCW-100 experiment, the second step was devoted to the stratification transient associated to an heavy metal formation at the bottom of the pool. Four different models were approximately calibrated and compared based on the experimental post-mortem analyses highlighting the needs for further work on the transient model validation.

In the near future, by the end of the CRP in mid-2024, this benchmark will be completed by a last step considering the transient evolution of a three-layer stratified corium pool in presence of a solid crust at the top oxide surface based the CORDEB2 CP7-02 experimental results.

ACKNOWLEDGMENTS

Authors would like to acknowledge the IAEA for the coordination of this CRP and in particular Mr Miassoedov from the Division of Nuclear Power and Mr Massara and Ms Veneau from the Division of Nuclear Installation Safety.

REFERENCES

- [1] F. Fichot, L. Carénini, N. Bakouta, H. Esmaili, L. Humphries, T. Laato, R. Le Tellier, L. Saas, I. Melnikov, P. Pandazis, S. Weber, R. J. Park, A. Philippov, and V. Strizhov, “Elaboration of a Phenomena Identification Ranking Table (PIRT) for the modelling of In-Vessel Retention,” *Annals of Nuclear Energy*, 146, 107617, 2020.
- [2] D. F. Tsurikov, V. F. Strizhov, S. V. Bechta, V. N. Zagriazkin and N. P. Kiselev, *Main Results of MASCA1 and 2 Projects*, Technical Report, RRC Kurchatov Institute, 2007.
- [3] V.G. Asmolov, S.S. Abalin, Yu.A. Veselkin, V.Yu. Vishnevsky, V.V. Vlasov, B.L.Gershman, Yu.G. Degaltsev, Ye.K. Dyakov, J.F. Isaev, A.N. Kiselev, N.P. Kiselev, A.M.Kovalev, A.G. Ol'khovsky, K.V. Pechalin, LM. Semenov, V.F. Strizhov, T.V.Trushkina, V.S. Uglov, Yu.M. Utkin, V.V.Chudanov, A.E.Aksenova, V.A.Pervichko and L.M. Khazanivich, *RCW Post-Test Analysis Results*, Technical Report MP-TR-11, Russian Research Centre Kurchatov Institute, 2003.
- [4] F. Fichot, B. Michel, L. Carénini and V. Almjashev, “Final report on stratified corium pool behaviour – CORDEB-2 tests”, Deliverable D3.2 of H2020 IVMR project, December 2019.

- [5] S. V. Bechta, V. S. Granovsky, K. V. B, V. V. Gusarov, V. I. Almiyashev, L. P. Mezentseva, E. V. Krushinov, S. Yu. Kotova, R. A. Kosarevsky, M. Barrachin, D. Bottomley, F. Fichot, and M. Fischer, "Corium Phase Equilibria based on MASCA, METCOR and CORPHAD Results," *Nuclear Engineering and Design*, vol. 238, pp. 2761–2771, 2008.
- [6] V. G. Asmolov, V. N. Zagryazkin, and D. F. Tsurikov, "Estimation of the density of U-Zr-Fe-O melts," *High Temp*, vol. 46, no. 4, pp. 579–582, Aug. 2008.
- [7] M. Barrachin and F. Defoort, Thermophysical Properties of In-Vessel Corium: MASCA Programme Related Results, Proc. Of MASCA Seminar, Aix-en-Provence, France, 2004.
- [8] M. A. Golubev, I. A. Melnikov, G. B. Shmelkov, A. V. Velikanov, "Thermodynamic model of the corium for NPP with VVER" in Proc. of XXIII Int. Conf. of Nuclear Power Plants, National Research Center "Kurchatov Institute", Moscow, Russia, 2023 (in russian).
- [9] M. Salay and F. Fichot, "Modelling of Metal-Oxide Corium Stratification in the Lower Plenum of a Reactor Vessel," in Proc. of Int. Topical Meeting on Nuclear Thermal-Hydraulics (NURETH-11), Avignon, France, 2005.
- [10] V. D. Ozrin, O. V. Tarasov, V. F. Strizhov, and A. S. Filippov, "A model for calculating composition and density of the core melt in the water-moderated water-cooled reactor in case of severe accident," *Therm. Eng.*, 57, 13, 1099–1111, 2010.
- [11] B. Sundman, U. R. Kattner, C. Sigli, M. Stratmann, R. Le Tellier, M. Palumbo, and S. G. Fries, "The OpenCalphad thermodynamic software interface," *Computational Materials Science*, 125, 188–196, 2016.
- [12] S. Bakardjieva, M. Barrachin, S. Bechta, D. Bottomley, L. Brissoneau, B. Cheynet, E. Fischer, C. Journeau, M. Kiselova, L. Mezentseva, P. Piluso, and T. Wiss, "Improvement of the European thermodynamic database NUCLEA," *Progress in Nuclear Energy*, 52, 1, 84–96, 2010.
- [13] S. Nandan, F. Fichot, and B. Piar, "A simplified model for the quaternary U-Zr-Fe-O system in the miscibility gap," *Nuclear Engineering and Design*, 364, 110608, Aug. 2020.
- [14] J. Mativet, R. Le Tellier, and A. Lecoanet, Improvement of thermochemical corium stratification modelling accounting for uranium and zirconium composition difference in metallic and oxide phases, in Proc. of the 11th European Review Meeting on Severe Accident Research Conference (ERMSAR 2024), KTH, Stockholm, Sweden, May 13-16, 2024.
- [15] G. Ratel, F. Deffort, K. Froment, B. Tourniaire and J. M. Seiler, Considerations on mass transfer kinetics for layer inversion and layer oxidation: from MASCA program to the reactor situation. Proc. of MASCA-2 Seminar, Cadarache, France 2007.
- [16] L. Carénini and F. Fichot, "Evaluation of the kinetics of molten pool stratification in case of In-Vessel Melt Retention Strategy," in Proc. of 26th International Conference on Nuclear Engineering ICONE 26, London, England, 2018.
- [17] R. Le Tellier, L. Saas and S. Bajard, Transient Stratification Modelling of a Corium Pool in a LWR Vessel Lower Head, *Nuclear Engineering and Design*, 287, 68-77, 2015.
- [18] R. Le Tellier, "Mass transfer between a continuous oxide phase (U-O-Zr) and a steel droplet at liquid state: Potential impact on corium pool behaviour during in-vessel melt retention," *Nuclear Engineering and Design*, 385, 111525, 2021.
- [19] R. Le Tellier, "A lumped parameter model of continuous/dispersed phases mass transfer for simulating in-vessel corium stratification transients," *Annals of Nuclear Energy*, 181, 109539, 2023.
- [20] F. Fichot, L. Carénini, R. Le Tellier, L. Viot, N. and Bakouta, and A. Filippov, "Identification and evaluation of the remaining uncertainties for transient situations," in Proc. of International Seminar "In-vessel retention: outcomes of IVMR project," Juan-les-Pins, France, Jan. 2020.

APPENDIX A: Results

Table VI. Step-1, C1 calculations: experimental values for the oxide phase mass fraction w^{oxy} , the U (resp. Zr) mass fraction in the metal phase w_U^{met} (resp. w_{Zr}^{met}) and relative difference (%) for the different codes and models. Cell colors correspond to the error range (green $\leq 5\% \leq$ yellow $\leq 10\% \leq$ orange $\leq 15\% \leq$ red).

		Experimental value	5	6	7	8	2	3	1	4
			CEA - PROCOR - NUCLEA	CEA - PROCOR - S&F	CEA - PROCOR - N&F	CEA - PROCOR - closures	IRSN - ASTEC	INRNE - ASTEC	NRC KI - TSAR	IBRAE - HEFEST_URAN
MA-1	w^{oxy}	0.781	-2.4%	-1.6%	-3.1%	-1.0%	1.0%	1.0%	4.2%	-2.7%
	w_U^{met}	0.425	-5.9%	-1.9%	0.1%	-14.2%	-8.3%	-8.1%	-2.9%	-10.7%
	w_{Zr}^{met}	0.103	34.0%	6.5%	8.7%	35.3%	-0.5%	-0.3%	36.3%	24.5%
MA-2	w^{oxy}	0.878	-3.4%	-2.5%	-3.7%	-3.0%	-1.3%	-1.4%	1.6%	-1.9%
	w_U^{met}	0.201	16.2%	10.5%	17.0%	-6.5%	-2.8%	-1.6%	-4.9%	-14.4%
	w_{Zr}^{met}	0.055	66.2%	21.0%	28.1%	66.4%	6.4%	7.8%	69.9%	-15.0%
MA-3	w^{oxy}	0.726	1.9%	3.1%	1.6%	4.0%	5.3%	5.2%	8.0%	4.5%
	w_U^{met}	0.430	-3.5%	-0.0%	1.5%	-12.5%	-3.7%	-3.6%	-5.5%	-10.1%
	w_{Zr}^{met}	0.173	-1.5%	-16.9%	-15.6%	1.3%	-19.9%	-19.9%	4.0%	-21.8%
MA-4	w^{oxy}	0.639	-3.2%	-3.3%	-2.9%	-0.3%	-0.2%	-0.2%	6.3%	-2.2%
	w_U^{met}	0.322	9.8%	15.9%	14.8%	0.3%	11.1%	11.1%	5.9%	-0.7%
	w_{Zr}^{met}	0.158	-9.9%	-23.0%	-23.7%	-9.0%	-26.2%	-26.1%	-3.1%	-10.7%
MA-5	w^{oxy}	0.754	-7.6%	-6.6%	-7.1%	-4.7%	-3.7%	-3.7%	-0.5%	-3.1%
	w_U^{met}	0.374	21.9%	26.2%	26.0%	12.4%	22.9%	23.0%	16.4%	18.6%
	w_{Zr}^{met}	0.256	-11.7%	-20.3%	-20.5%	-9.3%	-22.4%	-22.3%	-0.4%	-35.9%
MA-5b	w^{oxy}	0.799	-7.0%	-5.3%	-6.6%	-4.2%	-2.8%	-2.9%	-1.4%	-3.9%
	w_U^{met}	0.428	15.3%	18.7%	19.3%	6.5%	16.1%	16.2%	10.4%	16.3%
	w_{Zr}^{met}	0.274	-12.7%	-20.9%	-20.5%	-9.7%	-22.6%	-22.5%	-1.5%	-37.7%
MA-6	w^{oxy}	0.565	-9.6%	-11.3%	-8.1%	-13.6%	-7.9%	-7.2%	2.4%	-7.7%
	w_U^{met}	0.215	30.7%	41.3%	35.0%	41.2%	35.1%	35.2%	21.0%	16.7%
	w_{Zr}^{met}	0.142	-18.1%	-28.6%	-31.8%	-15.7%	-31.8%	-31.7%	-12.2%	-19.9%

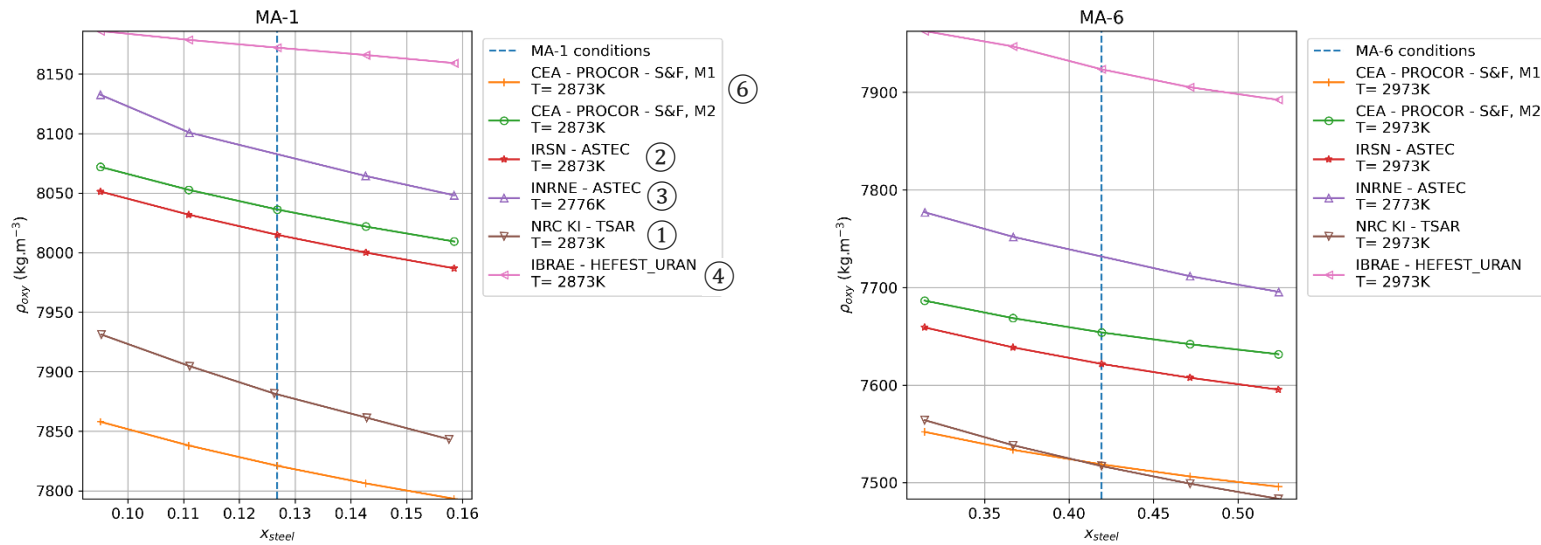


Figure 4. Step -1, C2 calculations: oxide phase density ρ^{oxy} as a function of x_{steel} in MA-1 (left) and MA-6 cases – circled numbers in the legend refer to the code/model numbering of Table III.

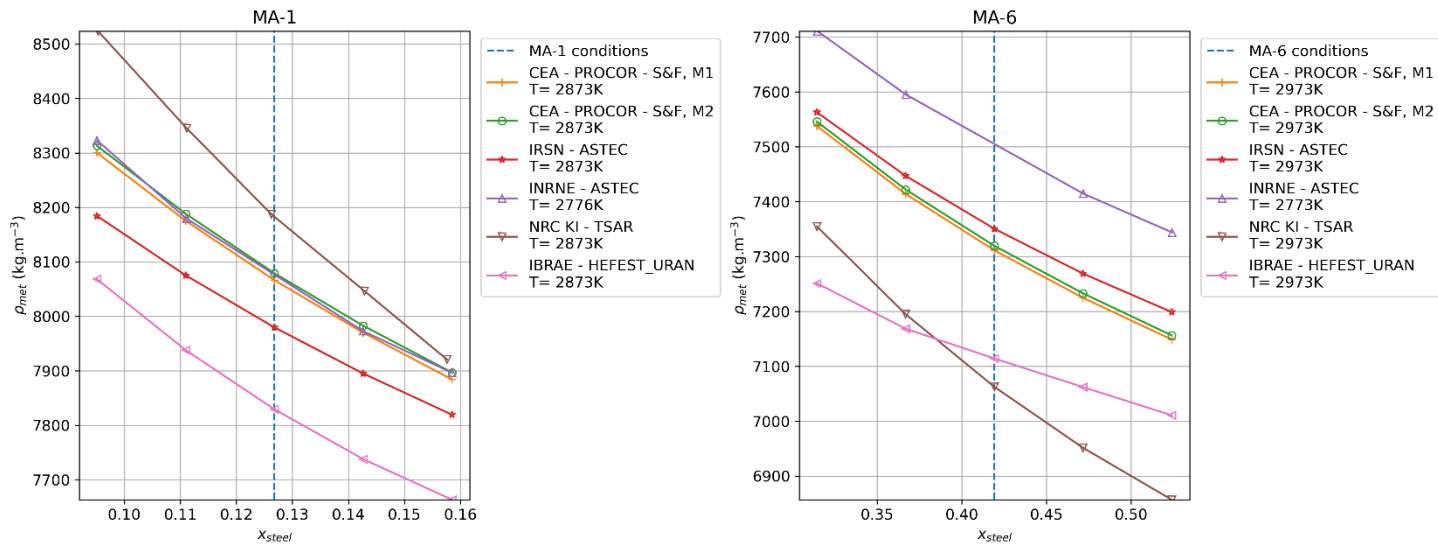


Figure 5. Step -1, C2 calculations: metal phase density ρ^{met} as a function of x_{steel} in MA-1 (left) and MA-6 cases.

Table VII. Step-1, C2 calculations: phase density difference $\rho^{met} - \rho^{oxy}$ [kg.m⁻³] for $x_{steel} = x_{steel}^{exp}$.

	6	6	2	3	1	4
	CEA - PROCOR - S&F, M1	CEA - PROCOR - S&F, M2	IRSN - ASTEC	INRNE - ASTEC	NRC KI - TSAR	IBRAE - HEFEST_URAN
MA-1	245.3	42.8	-35.3	-91.4	305.6	-342.9
MA-2	-559.3	-763.2	-771.1	-785.6	-717.3	-1075.9
MA-3	503.3	316.1	315.4	316.1	543.6	-68.3
MA-4	183.6	-7.6	-4.5	-50.5	64.8	-489.1
MA-5	907.3	740.9	712.7	721.0	794.0	542.4
MA-5b	1100.8	937.7	927.0	936.2	955.1	984.1
MA-6	-207.4	-334.4	-271.1	-296.8	-454.4	-809.3

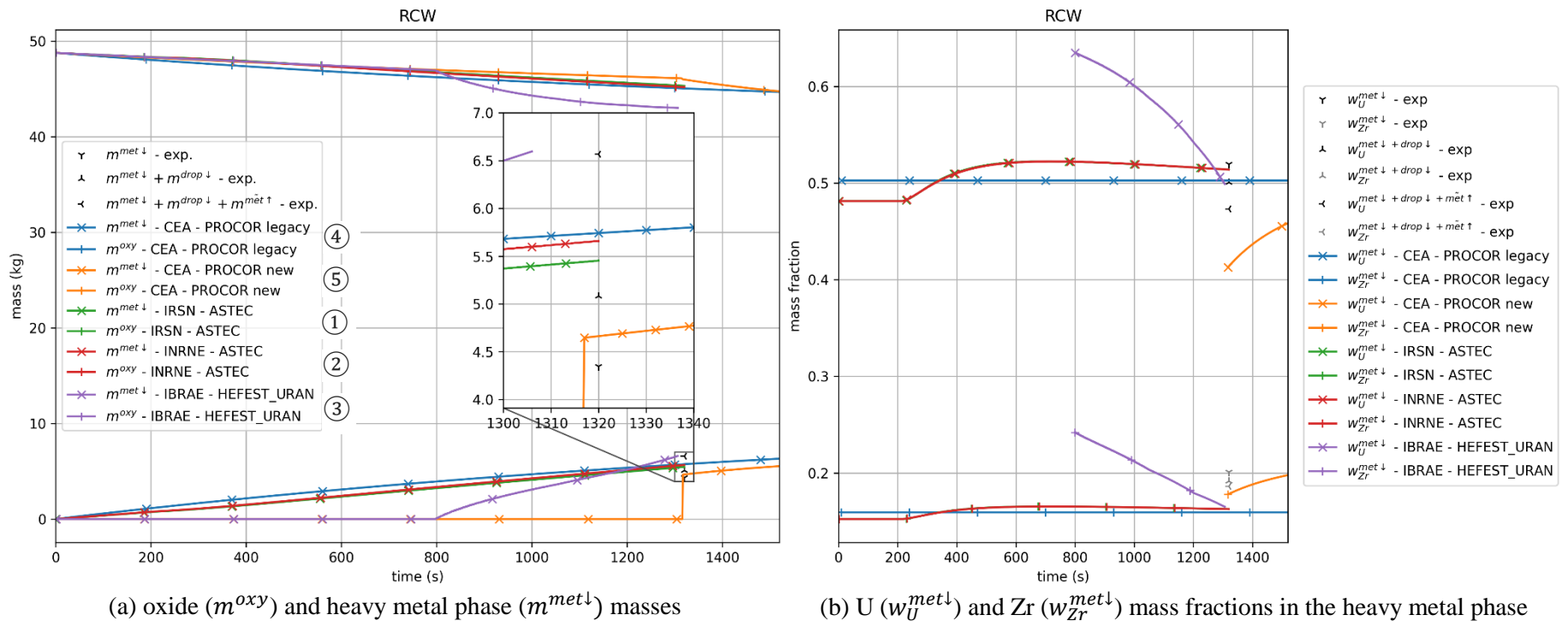


Figure 6. Step-2: phase masses and heavy metal phase composition evolution for the different simulations and comparison with experimental values – circled numbers in the legend refer to the code/model numbering of Table V.